Internal conversion coefficients in ^{134}Cs, ^{137}Ba, and ^{139}La: A precise test of theory

N. Nica,* J. C. Hardy, V. E. Iacob, and C. Balonek†
Cyclotron Institute, Texas A&M University, College Station, Texas 77843, USA‡

M. B. Trzhaskovskaya
Petersburg Nuclear Physics Institute, Gatchina, RU-188300, Russia
(Received 14 January 2008; published 14 March 2008)

Recently we measured the ratio of K-shell internal conversion coefficients, α_K, for the 127.5-keV $E3$ transition in ^{134}Cs and the 661.7-keV $M4$ transition in ^{137}Ba. We here report a measurement of the 165.9-keV $M1$ transition in ^{139}La, based on which we convert our earlier ratio measurement into individual α_K values for the transitions in ^{134}Cs and ^{137}Ba. These results continue to confirm the Dirac-Fock calculations of internal conversion coefficients that incorporate the atomic K-shell vacancy.

DOI: 10.1103/PhysRevC.77.034306 PACS number(s): 23.20.Nx, 27.60.+j

I. INTRODUCTION

Although internal conversion is an important component of most nuclear decay schemes, until recently the accuracy of calculated internal conversion coefficients (ICCs) was, at best, ill defined. How could it be otherwise, since there were very few precise measurements of ICCs in existence, against which the calculated results could be tested. In 1973 Raman *et al.* [1] compared "precisely measured" ICCs for 15 $E3$ and $M4$ transitions with the tabulated Hager and Seltzer calculations [2] and concluded that the theoretical values were systematically higher by 2–3%. However, even this select group of transitions included only five with measured ICCs that were known with a precision of 2% or better, so the apparent discrepancy was hardly definitive. Yet this is where the matter remained for 30 years.

By 2002 Raman *et al.* [3] had 100 experimental ICCs to compare with tabulated values, but even at that recent date only 20 of the measured ICCs had a precision of 2% or better. Their results still indicated that all previous tables of ICCs exhibited a 3% systematic bias, but the authors found much better agreement (within ∼1%) for a new table by Band *et al.* [4], which was calculated in the framework of the Dirac-Fock method and, for the first time, treated the exchange between electrons exactly. Yet, even though the average agreement was now much better, some of the individual ICCs disagreed significantly from the calculated values, and, even more troubling, the data appeared to show a surprising preference for one particular model in which the final-state electron wave function was computed in a field that did not include the atomic subshell vacancy caused by the conversion process.

The question of whether to include the atomic vacancy was settled in 2004 by our precise measurement (±0.8%) of the K-shell conversion coefficient, α_K, for the 80.2-keV $M4$ transition in ^{193}Ir [5,6]. The impact of that result is illustrated in Fig. 1, where we plot differences between 21 experimental ICCs and two versions of the Dirac-Fock theory (see Refs. [3,5]), one that ignores the atomic vacancy and the other that includes it via the "frozen orbital" approximation. In addition to our ^{193}Ir result, the figure includes the 20 cases with better than 2% precision, which were listed by Raman *et al.* [3] in 2002. Clearly the ^{193}Ir result leaves little doubt that the atomic vacancy must be incorporated in the ICC calculation. Even so, there are still a number of the previously measured cases that agree less well with the vacancy calculation, and there are even several cases—two $E3$ transitions (a 40-keV one in ^{103}Rh and a 128-keV one in ^{134}Cs) and a 347-keV $M4$ transition in ^{197}Pt—that differ by more than two standard deviations from both types of calculation. If taken at face value, these three discrepant cases could indicate that some further aspect of the theory is not quite complete.

In a recent paper [7], we reported a measurement of one of these discrepant cases, the $E3$ transition in ^{134}Cs, in which its α_K was obtained relative to that of the 662-keV $M4$ transition in ^{137}Ba (also identified in Fig. 1). The measured ratio was compared with the calculated results from two versions of the Dirac-Fock theory; it agreed well with the version that included the atomic vacancy and deviated significantly from the other. However, that measurement did not yield individual results for each transition's α_K value. We now report a measurement on a 166-keV $M1$ transition in ^{139}La, which allows us to extract from our previous data the individual α_K values for the transitions in both ^{134}Cs and ^{137}Ba.

II. MEASUREMENT OVERVIEW

We have described our measurement techniques in detail in previous publications [5,7] so only a summary will be given here. If a decay scheme is dominated by a single transition that can convert in the atomic K shell, and a spectrum of K x rays and γ rays is recorded for its decay, then the K-shell internal conversion coefficient for that transition is given by

$$\alpha_K \omega_K = \frac{N_K}{N_\gamma} \cdot \frac{\epsilon_\gamma}{\epsilon_K}, \tag{1}$$

*nica@comp.tamu.edu
†REU summer student from State University of New York at Buffalo, Buffalo, NY.
‡http://cyclotron.tamu.edu/
‡krutov@ssu.samara.ru

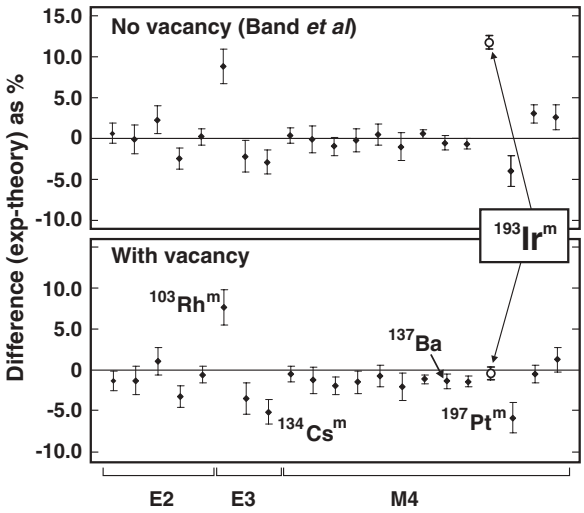

FIG. 1. Percentage differences between the measured and calculated ICCs for two Dirac-Fock calculations: one (top) is without the atomic vacancy and the other (bottom) is with it included in the "frozen orbital" approximation. The points shown as solid diamonds in both plots correspond to the 20 cases listed by Raman *et al.* [3] that have better than 2% precision; as indicated at the bottom, five are for $E2$ tranditions, three for $E3$, and the remainder are for $M4$ transitions. The points shown as open circles correspond to the more recently measured α_K value for ^{193}Ir [5,6].

where ω_K is the fluorescence yield; N_K and N_γ are the total numbers of observed K x rays and γ rays, respectively; and ϵ_K and ϵ_γ are the corresponding detector efficiencies. Fluorescence yields have been well measured for cesium, barium, and lanthanum [8]. They have also recently been evaluated as a function of Z [9] for all elements with $10 \leqslant Z \leqslant 100$, and ω_K values have been recommended, which have an uncertainty of about 0.5% around $Z = 55$. Thus, in the mass region of interest here, Eq. (1) allows α_K to be extracted directly from measured peak areas with subpercent precision provided that the detector efficiencies are sufficiently well known.

In our experiments, we detect both the γ ray and the K x rays in the same high-purity germanium (HPGe) detector, a detector whose efficiency has been meticulously calibrated [10–12] to subpercent precision between 50 and 3500 keV. Thus, when both peaks lie within this range, the efficiency ratio, $\epsilon_\gamma/\epsilon_K$, in Eq. (1) can be quoted to the same high precision. However, the K x rays from cesium, barium, and lanthanum lie between 30 and 40 keV, significantly below that range, so here we can only achieve high precision by measuring the ratio of K-conversion coefficients for two independent transitions in nuclei with similar x-ray energies. If we denote the two transitions by subscripts 1 and 2, and apply Eq. (1) to both, the ICC ratio is given by

$$\frac{\alpha_{K1}}{\alpha_{K2}} = \frac{\omega_{K2}}{\omega_{K1}} \cdot \frac{N_{K1}N_{\gamma 2}}{N_{\gamma 1}N_{K2}} \cdot \frac{\epsilon_{\gamma 1}}{\epsilon_{\gamma 2}} \cdot \frac{\epsilon_{K2}}{\epsilon_{K1}}. \qquad (2)$$

Here the efficiencies in the K x-ray region, ϵ_{K1} and ϵ_{K2}, appear only in a ratio.

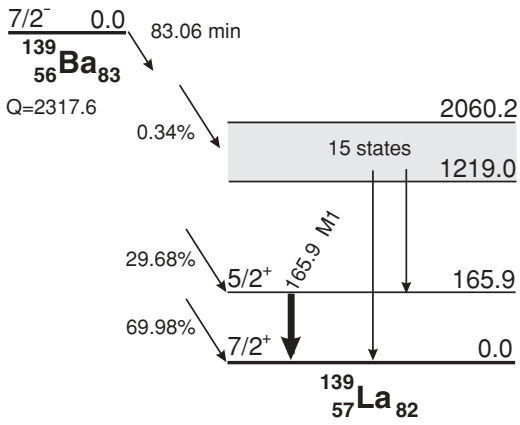

FIG. 2. Abbreviated decay scheme for the β decay of ^{139}Ba. The information is taken from Ref. [13]. Note that all known γ-ray transitions from the 15 excited states populated in β decay go directly to the ground or first-excited state of ^{139}La.

In the 30–40-keV range, the efficiency of our detector changes by only 0.38%/keV, a small amount whose uncertainty is completely negligible in the context of Eq. (2) if the x-ray energies are within a few keV of one another. This was the case for our recent measurement of the α_K ratio for the transitions in $^{134}_{55}$Cs and $^{137}_{56}$Ba [7]. There we determined the ratio to a precision of 0.5% and compared that result to theoretical ratios calculated with various methods for dealing with the atomic vacancy. Although our result agreed with the calculation that included the vacancy, it could not in itself resolve the discrepancies evident in Fig. 1 for both ^{134}Cs and ^{137}Ba: though the ratio agreed with theory, it was still possible that both α_K values individually disagreed with the calculated values.

We describe in this paper an experimental study of the 165.8576(11)-keV $M1$ transition from the first-excited state of $^{139}_{57}$La [13], which produces x rays with energies very close to those from cesium and barium. We isolated this transition by observing it following the β decay of 83-min ^{139}Ba. The decay scheme is shown in Fig. 2, where it can be seen that the 165.9-keV transition is the dominant one resulting from this β decay. The total strength of all other transitions produced in ^{139}La is two orders of magnitude less, and, all being of significantly higher energy, their K-shell conversion is down by another two orders. Thus the K x rays observed following the ^{139}Ba β decay are more than 99.9% due to the 165.9-keV transition in ^{139}La.

This transition is also known to have essentially pure $M1$ multipolarity [14] and a $B(M1)$ of 0.00257 Weisskopf units [13], which is well within the range of nonhindered transitions. Under these conditions, the value of α_K can be reliably calculated. Moreover, unlike the $E3$ and $M4$ transitions in ^{134}Cs and ^{137}Ba, the α_K value for the ^{139}La transition is essentially independent of how the atomic vacancy is handled in the calculation, being 0.2231 if the vacancy is included and 0.2226 if it is not. Consequently, we can use 0.2229(3) as a "method-independent" α_K value for the transition.

The goal of our experiment then was to measure precisely the N_K/N_γ ratio for the ^{139}La transition. With this result and

the unambiguously calculated α_K value for that transition, we could next apply Eq. (2) to obtain an individual α_K value for the previously measured transitions in both ^{134}Cs and ^{137}Ba. For example, if in Eq. (2) we were to label the ^{134}Cs transition "1" and the ^{139}La transition "2", then we could solve for α_{K1}, the ICC for the ^{134}Cs transition, since all other quantities, including α_{K2}, would be known. In effect, we would be using the ^{139}La measurement to calibrate our detector's efficiency at the relevant x-ray energies and then applying that efficiency to reanalyze our previous results for the transitions in ^{134}Cs and ^{137}Ba. With individual α_K values determined for both those transitions, it would become possible to compare them with theory and resolve (or not) the discrepancies evident in Fig. 1.

III. EXPERIMENT

Because the present result was to be combined with results from our previous measurement on ^{134}Cs and ^{137}Ba [7], we followed as closely as possible the same approach. Only those details not covered previously will be described here.

We produced ^{139}Ba by neutron activation of ^{138}Ba. Because of its short, 83-min half-life, we chose to prepare a uniform layer of material, suitable for a thin source, and irradiate it in that form, rather than irradiating the material first and preparing a source later. As material, we used $Ba(NO_3)_2$, enriched in ^{138}Ba.[1] We placed a 0.05-ml drop of an aqueous solution containing 126 μg of $^{138}Ba(NO_3)_2$ onto a layer of 1/10 diluted wet insulin on a substrate of 12-μm-thick Mylar. It was then dried and examined under a microscope. Of eight samples prepared in this way, we selected two as being the most uniform, with a sample layer averaging 1 μm thick. The two selected samples were finally covered with 4-μm-thick Mylar and designated T1 and T2.

Two separate irradiations were made. For each, the sample to be activated was placed in a thermal neutron flux of $\sim 7 \times 10^{12}$ n/cm^2 s at the TRIGA reactor in the Texas A&M Nuclear Science Center. In the case of T1, the exposure time was 1.8 h; for T2, it was 1 h. After removal from the reactor, each Mylar assembly was trimmed to a disk, 13 mm in diameter, with the contained radioactive spot being 7 mm in diameter.

We acquired spectra from both sources using the same equipment and procedures as we have described in a previous publication [5]. In all, we obtained nine spectra from the T1 source (labeled T1.1 through T1.9) and eight from T2 (T2.1 through T2.8). All spectra covered the energy interval 10–2000 keV with a dispersion of about 0.25 keV/channel. The first five spectra with source T1 and the first four with T2 were taken within 6 h of the irradiation ($\sim$4.5 half-lives of ^{139}Ba). The remaining spectra were obtained over an extended period of time (in one case after 6 days) so that we could confidently identify and correct for all relevant impurities.

[1]This material was obtained from our laboratory inventory; unfortunately, its exact enrichment had not been recorded. However, we saw no evidence of any barium contaminants in our γ-ray spectra.

IV. ANALYSIS

In our analysis of the data, we followed the same methodology as we did with previous source measurements [5–7]. We first extracted areas for all the x- and γ-ray peaks of interest. Next, we identified impurities and made appropriate corrections to account for their effects on the peaks required for the determination of α_K. Finally, we dealt with the various small corrections that had to be applied to these peak areas to account for competing transitions, x-ray scattering, and the non-Gaussian shape of the x-ray peaks themselves.

A. Peak areas

The spectra in Fig. 3 show the energy regions of primary interest for this measurement, one encompassing the K x rays, and the other the 165.9-keV γ ray. As before [5–7], we determined all peak areas with GF2, the least-squares peak-fitting program in the RADWARE series [15]. In doing so, we used the same fitting procedures as were used in the original detector-efficiency calibration [10–12]. This was particularly straightforward for the γ-ray peak, since it lies on a flat background, well isolated from any other peaks, and with no evidence of competing impurities.

However, the x-ray region is not so simple, and although the impurity contribution turns out to be relatively small (see Sec. IV B), it must be carefully accounted for in our analysis. We extracted areas from the x-ray region by integrating the total area of the combined K_α and K_β groups between equivalent energy limits. We used a special modification [15] of the GF2 program that allows us to set a background by the normal fitting procedures and then to integrate the total number of counts above that background within set limits, extrapolating a Gaussian tail to account for counts possibly outside those limits.

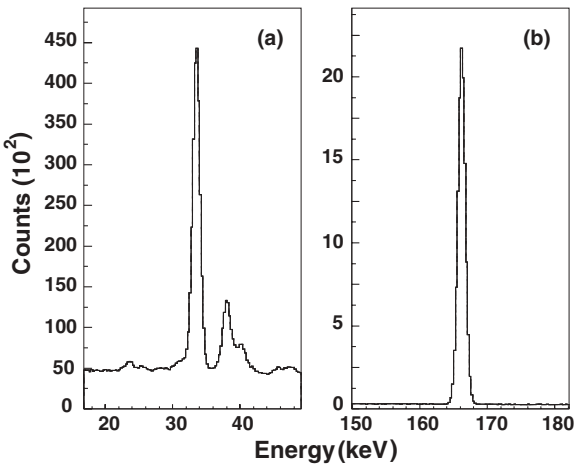

FIG. 3. Spectra for the two energy regions of interest in the determination of the α_K ratio for the 165.9-keV transition in ^{139}La: (a) the lanthanum K x rays and (b) the 165.9-keV γ ray.

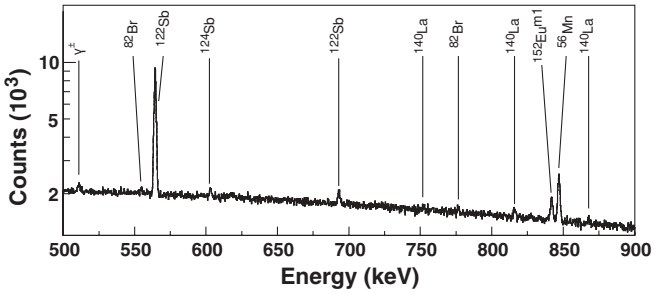

FIG. 4. Portion of the γ-ray energy spectrum T1.1, measured soon after the activation of source T1. Peaks are identified by their β-decay parent.

B. Impurity identification

We observed a number of weak impurities in our sources, some coming from the sample itself and some from the Mylar substrate. As a typical example, a portion of one of our 17 γ-ray spectra appears in Fig. 4 with contaminant peaks identified. As is evident there, even the weakest peaks were identified; this same procedure was followed for all recorded spectra. After careful analysis of all recorded spectra for contaminants, we identified four activities of concern to our evaluation of the lanthanum K x rays: ^{80}Br^m, ^{140}La, ^{152}Eu^{m1}, and ^{153}Sm. In addition, we observed ^{24}Na, ^{56}Mn, ^{82}Br, ^{122}Sb, and ^{181,185}Os, which do not interfere with our peaks of interest, and negligible traces of other impurities whose contributions total considerably less than 0.1%. In dealing with the important impurities, we obtained the contribution of each to the lanthanum K x-ray peak region as a function of time based on the observed intensities of γ rays from that same impurity observed elsewhere in the spectrum. Then, using these contributions and the known half-life of each impurity, we derived the activity of each at time $t = 0$, which we defined to be the time when the neutron activation ended. We will briefly describe our handling of each important impurity in turn.

$^{80}Br^m$. In our previous measurement [7], which also used Mylar substrates, we noted the presence of both ^{80}Br^m ($t_{1/2} =$ 4.4 h) and ^{82}Br ($t_{1/2} = 35.3$ h) produced from small amounts of bromine in the foil. It is ^{80}Br^m that causes a problem, since its decay comprises a single observable γ-ray peak at 37.1 keV, which in this measurement would be unresolved from the lanthanum K_β peaks. However, since we have already measured [7] the relative intensities of the ^{80}Br^m peak and the ^{82}Br peaks at 554.3 and 776.5 keV as a function of time after activation, we could analyze our spectra from sources T1 and T2 using the relatively strong peaks from ^{82}Br to calculate with good accuracy the intensity of the 37.1-keV γ ray. The result is given in Table I where it is expressed as a percentage of the total uncorrected activity of the summed lanthanum ($K_\alpha + K_\beta$) x-ray peaks.

^{140}La. We observed two pronounced γ rays—at 487.0 and 1596.2 keV—from the decay of 1.68-d ^{140}La, which was apparently produced from a lanthanum impurity in our barium nitrate sample. (Three weaker peaks from the same decay are identified in Fig. 4.) Since the β decay of ^{140}La populates states in ^{140}Ce, our concern was for the cerium K x rays, because they cannot be resolved from the lanthanum x rays of interest. Based on the observed γ rays, their decay with time, and the tabulated properties of the decay scheme [16], we determined

TABLE I. Results for the 165.9-keV transition in ^{139}La, including some applied corrections. The top part of the table lists the impurities that can contribute to the summed ($K_\alpha + K_\beta$) x-ray peaks, with the last two columns giving the sizes of the contributions immediately after activation for the two sources, T1 and T2, expressed as a percentage of the respective corrected activities. Decay rates in the bottom part of the table are also referred to $t = 0$, the time that the neutron activation concluded. Additional corrections for scattering and for the Lorentzian shape of the x-ray peaks are applied to the results in Tables II and III.

		Source	
		T1	T2
Contaminant activities:			
^{80}Br^m	37.1-keV γ ray	1.13(1)%	1.39(2)%
^{140}La	Ce ($K_\alpha + K_\beta$)	0.08(1)%	0.07(1)%
^{152}Eu^{m1}	(Sm + Gd)K_α	3.69(3)%	2.88(3)%
^{153}Sm	Eu K_α	0.72(2)%	0.51(1)%
Total impurities		5.62(4)%	4.85(4)%
Contaminant-corrected rates:			
($K_\alpha + K_\beta$) decay rate (s^{-1})		217.3(9)	182.8(10)
165.9-keV γ-ray decay rate (s^{-1})		898.2(13)	759.8(15)
Ratio, N_K/N_γ		0.2419(10)	0.2406(14)
Average N_K/N_γ		0.2414(8)	
Attenuation in source:			
Relative x-ray attenuation		0.19(2)%	
Corrected ratio, N_K/N_γ		0.2419(8)	

the total intensity of the cerium K x rays at $t = 0$. The result is given in Table I.

$^{152}Eu^{m1}$. Evidently europium was another impurity in our barium nitrate sample, since we also observed γ rays at 121.8, 841.6, and 963.4 keV from the 9.3-h decay of $^{152}Eu^{m1}$. (The second of these γ rays is identified in Fig. 4.) The decay of $^{152}Eu^{m1}$ proceeds both by β^- emission (27%) to ^{152}Gd and by β^+ and electron capture (73%) to ^{152}Sm, producing x rays characteristic of gadolinium and samarium. The K_α peaks from both these elements interfere with the high-energy side of our lanthanum K_β peaks. Here again we used the observed γ rays, their decay, and the tabulated properties of the $^{152}Eu^{m1}$ decay [16] to determine the total intensity of the gadolinium and samarium K_α x rays at $t = 0$. As shown in Table I, at ~3% this was the strongest contamination affecting the lanthanum x rays.

^{153}Sm. The last impurity of significance was 46.3-h ^{153}Sm, which β^- decays to ^{153}Eu, giving rise to europium x rays. As was true for the x rays from gadolinium and samarium, the K_α peak from europium also interferes with the high-energy side of our lanthanum K_β peaks. We used the observed 103.2-keV γ-ray peak from the ^{153}Sm decay to determine the intensity of the associated europium K_α peak at $t = 0$, and this result is presented in Table I.

C. Half-life analysis

Once the impurities had been identified and their intensities in the region of the lanthanum K x rays determined, we subtracted their contribution from the total area of the combined K_α and K_β groups in each spectrum. The resulting areas, expressed as decay rates, are plotted as a function of time in Fig. 5 for both sources. Unfortunately, there is considerable scatter in existing measurements of the half-life of ^{138}Ba [13], with six published values spanning a range from 82.5 to 85.0 min, so we decided to use our own data on the decay of the 165.9-keV γ ray to determine the half-life we would use to analyze the x rays.

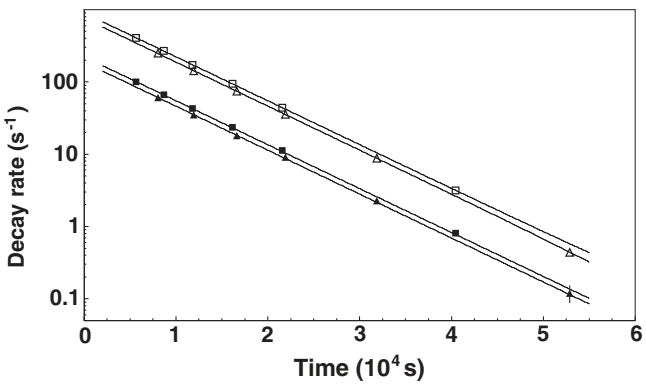

FIG. 5. Decay rates for the lanthanum K x rays and the 165.9-keV γ rays from both sources. The squares refer to source T1 and the triangles to T2; open symbols are for the γ ray, and solid ones for the x rays. The lines through the points are best fits to the data as described in the text. The zero of the time axis corresponds to the end of the neutron activation period. Note that the results from spectra taken at later times were consistent with zero and were not included in the plot area.

As was noted in Sec. IV A and is clear from Fig. 3, the 165.9-keV γ-ray peak areas presented no difficulties with either background or impurities. The results for their decay are also shown in Fig. 5. A least-squares fit to these points yielded a half-life of 82.60(8) min for the T1 source and 82.54(8) min for T2. The corresponding normalized χ^2 values were 0.2 and 1.7, respectively. Taking the average value and incorporating some provision for systematic uncertainty, we take 82.57(12) min to be the half-life for ^{138}Ba, a value that lies at the lowest end of the range of previous results. The fits also yielded decay rates evaluated at $t = 0$, and these are given in Table I.

With the half-life fixed at the value just obtained from the γ-ray decay, we performed another least-squares fit, this time to the decay of the summed K x rays. The normalized χ^2 values in both cases were less than 0.1, strongly supporting our prior treatment in removing contaminant activities, while suggesting that the uncertainties assigned to these corrections were, if anything, overestimated. The corresponding decay rates for the x rays at $t = 0$ also appear in Table I.

D. Attenuation in the sample

As described in Sec. III, our sources were activated barium nitrate in a layer ~1 μm thick, covered by a 4-μm-thick Mylar foil. For this configuration, we calculated the attenuation both of the lanthanum x rays and of the 165.9-keV γ ray using standard tables of attenuation coefficients [17]. The attenuation is very small, of course, with the x rays suffering 0.19(2)% more than the γ ray. This result is incorporated into Table I.

E. Scattering

In our recent publication on conversion coefficients in ^{134}Cs and ^{137}Ba [7], we discussed in detail the effects of scattered photons in creating a continuum, or shelf, that extends from the low-energy side of x-ray peaks. We studied this phenomenon with careful measurements, using HPGe and Si(Li) detectors, and with Monte Carlo calculations using the CYLTRAN code [18], the same code we had previously used in the precise calibration of our detector [10–12]. We demonstrated that the Monte Carlo calculation gave the correct energy dependence of the continuum and that it could therefore be used to determine what fraction of the total continuum lay hidden within the x-ray peak itself under experimental conditions. From the continuum actually observed at the low-energy side of the x-ray peak, it thus became possible to determine the number of scattered events that needed to be subtracted from the area of the peak itself.

We used exactly the same methodology to analyze the x-ray peaks in our ^{139}La spectra, which are only a few keV away from the cesium and barium x rays. The resulting correction for the combined lanthanum K_α and K_β x-ray peak areas was −1.9(3)%, which compares with the corrections we previously derived for the cesium and barium peak areas: −2.8(4)% and −2.1(3)%, respectively. Since the same method was used to

TABLE II. Evaluation of the α_K value for the 127.5-keV $E3$ transition in ^{134}Cs. The symbols and notation are the same as in Eq. (2).

Quantity	Value	Source
$N_{K1}/N_{\gamma 1}$ (^{134}Cs)	2.660(4)	Table I of Ref. [7]
$N_{K2}/N_{\gamma 2}$ (^{139}La)	0.2419(8)	Table I, this work
$(N_{K1}N_{\gamma 2})/(N_{\gamma 2}N_{K1})$	10.99(4)	
Scattering correction	−0.95(30)%	Sec. IV E
Fully corrected ratio	10.89(5)	
ω_{K2}/ω_{K1}	1.012(2)	[9]
$\epsilon_{\gamma 1}/\epsilon_{\gamma 2}$	1.106(2)	[11]
$\epsilon_{K2}/\epsilon_{K1}$	1.0093(3)	Sec. II
α_{K2}(^{139}La)	0.2229(3)	Sec. II
α_{K1}(^{134}Cs)	2.742(15)	

correct all three of these cases, the principal uncertainty in the correction is systematic to them all. As a result, we actually apply the correction to the x-ray ratios rather than to the individual peak areas, in which case the correction becomes −0.19(30)% for the Ba/La ratio and −0.95(30)% for Cs/La. These values are used in Tables II and III.

F. Lorentzian correction

As described in Sec. IV A, to be consistent with our previous efficiency-calibration procedures, we extracted our experimental peak areas using a special modification of the GF2 program that allows us to integrate the total counts above background within selected energy limits. To correct for possible missed counts outside those limits, the program adds an extrapolated Gaussian tail. We have noted in previous papers [5–7] that this extrapolated tail does not do full justice to x-ray peaks, whose shapes reflect the finite widths of the atomic levels responsible for them. As we did before, to correct for this effect we computed a simulated spectrum using realistic Voigt-function shapes for the x-ray peaks. Because we had analyzed the measured x-ray peaks as a group, in our simulation we generated the whole group with the tabulated relative x-ray intensities and then scaled them to the number of counts actually obtained in our experiment. The simulated spectrum was then analyzed with GF2 following exactly the same fitting procedure as was used for the real data. We could then compare the areas obtained by GF2 for the lanthanum x-ray peaks with the actual peak areas used in the simulations. We found that 0.13% of the x-ray peak area was lost, a small correction in itself but, being common to the x-ray peaks of cesium, barium, and lanthanum, completely negligible in any ratio. No correction for this effect was applied.

TABLE III. Evaluation of the α_K value for the 661.7-keV $M4$ transition in ^{137}Ba. The symbols and notation are the same as in Eq. (2).

Quantity	Value	Source
$N_{K1}/N_{\gamma 1}$ (^{137}Ba)	0.2559(6)	Table I of Ref. [7]
$N_{K2}/N_{\gamma 2}$ (^{139}La)	0.2419(8)	Table I, this work
$(N_{K1}N_{\gamma 2})/(N_{\gamma 2}N_{K1})$	1.058(4)	
Scattering correction	−0.19(30)%	Sec. IV E
Fully corrected ratio	1.056(5)	
ω_{K2}/ω_{K1}	1.006(2)	[9]
$\epsilon_{\gamma 1}/\epsilon_{\gamma 2}$	0.3846(8)	[11]
$\epsilon_{K2}/\epsilon_{K1}$	1.0044(3)	Sec. II
α_{K2}(^{139}La)	0.2229(3)	Sec. II
α_{K1}(^{137}Ba)	0.0915(5)	

V. RESULTS AND DISCUSSION

The bottom line of Table I gives the ratio N_K/N_γ for the 165.9-keV $M1$ transition in ^{139}La after correction for contaminants and attenuation in the source. The equivalent results for the 127.5-keV $E3$ transition in ^{134}Cs and the 661.7-keV $M4$ transition in ^{137}Ba appear as the bottom line of Table I in Ref. [7]. With Eq. (2) in mind, we can now process these results farther to extract the α_K conversion coefficients for the ^{134}Cs and ^{137}Ba transitions. The details are summarized in Table II for ^{134}Cs and in Table III for ^{137}Ba.

The fully corrected ratios, $(N_{K1}N_{\gamma 2})/(N_{\gamma 2}N_{K1})$, for the ^{134}Cs/^{139}La comparison and for ^{137}Ba/^{139}La appear in the fifth line of the tables. These are the values that can now be inserted into Eq. (2) in order to evaluate final α_{K1} values for the transitions in ^{134}Cs and ^{137}Ba. The other terms also required for that equation are listed in the subsequent four lines of the table, together with the sources from which they were obtained. In particular, for the fluorescence yields, individual values are quoted in Ref. [9] to 0.5% precision; however, the values themselves are demonstrated to vary smoothly as a function of Z, so the percentage uncertainty on the ratio of two neighboring elements, whose ω_K values differ by only 0.7%, must surely be considerably smaller than the individual uncertainties. We conservatively assigned an uncertainty of

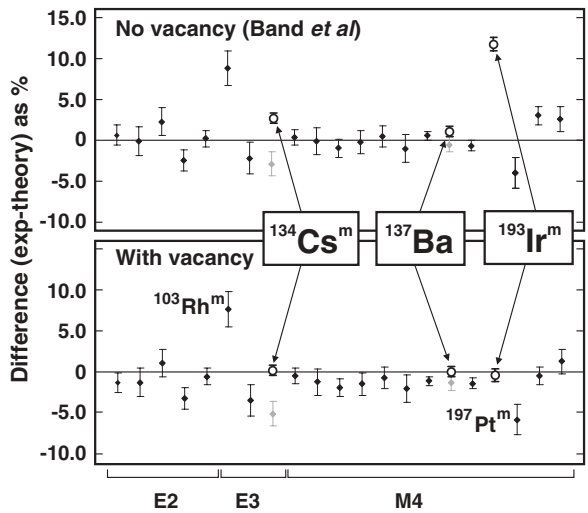

FIG. 6. Same as Fig. 1, except that the two results from the present work, for ^{134}Cs and ^{137}Ba, have been added as open circles. They both are seen to agree with the calculation that includes the atomic vacancy in the "frozen orbital" approximation. The previous values that were listed by Raman *et al.* [3] are shown in grey, slightly displaced.

TABLE IV. Comparison of the measured α_K values for the ^{134}Cs and ^{137}Ba transitions with calculated values based on different theoretical models for dealing with the K-shell vacancy. Shown also are the percentage deviations, Δ, from the experimental value. For a description of the various models used to determine the conversion coefficients, see Ref. [5].

	^{134}Cs		^{137}Ba	
	α_K	Δ(%)	α_K	Δ(%)
Experiment	2.742(15)		0.0915(5)	
Theory:				
No hole	2.677	2.4(5)	0.09068	0.9(5)
Hole, frozen orbitals	2.741	0.0(5)	0.09148	0.0(5)
Hole, SCF of ion	2.730	0.4(5)	0.09139	0.1(5)

0.2% to the ratio. Our final results for the α_K values are given in the last lines of Tables II and III.

In comparing this result to previous measurements, we refer to the recent survey [3] of world data on ICC values measured with an accuracy of better than 5%. The survey lists three previous measurements of α_K for the 127.5-keV transition in ^{134}Cs and ten for the 661.7-keV transition in ^{137}Ba. Unfortunately, in neither case are the measurements statistically consistent with one another: for the ^{134}Cs transition, the normalized χ-squared is 4.5; and for the one in ^{137}Ba, it is 3.7. What the reviewers opted to do was to "adopt" recommended values based on their critical evaluation of the individual measurements rather than take rigorous statistical averages, which would have had very large uncertainties. Their adopted values were $\alpha_K(^{134}\text{Cs}) = 2.60(4)$ and $\alpha_K(^{137}\text{Ba}) = 0.0902(8)$. Our result for ^{134}Cs is more than three standard deviations higher than the adopted value but more than twice as precise; our result for ^{137}Ba is also higher and more precise than the adopted value, but it is less than two standard deviations away. Under the circumstances, we choose not to average our results with previous measurements.

Our measured α_K values are compared with three different theoretical calculations in Table IV. All three calculations are made with the Dirac-Fock framework, but one ignores the presence of the K-shell hole, while the other two include it using different approximations: the frozen orbital approximation, in which it is assumed that the atomic orbitals have no time to rearrange after the electron's removal; and the SCF approximation, in which the final-state continuum wave function is calculated in the self-consistent field (SCF) of the ion, assuming full relaxation of the ion orbitals. The percentage deviations given in the table indicate excellent agreement with both calculations that include the effects of the atomic vacancy, and disagreement with the calculation that ignores the hole, by five standard deviations in the case of ^{134}Cs and by two in the case of ^{137}Ba.

This point is convincingly illustrated by Fig. 6, in which our measurements (open circles) are compared graphically with two of the calculations and with the previously accepted values (grey points). Where the previous ^{134}Cs α_K value disagreed with all theoretical values, it now agrees precisely with the calculations that include the atomic vacancy; and where the ^{137}Ba value previously supported the no-hole calculation, it too now favors the calculation with the hole included. In both cases, the uncertainties have been significantly reduced.

VI. CONCLUSIONS

By measuring the ratio of x rays to γ rays for the 165.9-keV $M1$ transition in ^{139}La, we have been able to convert our previous measurement of a ratio of α_K values into experimental results for the individual α_K values of the 127.5-keV $E3$ transition in ^{134}Cs and the 661.7-keV $M4$ transition in ^{137}Ba. Both of the latter transitions were of interest because their accepted α_K values either favored the no-vacancy model for the internal-conversion process or did not agree with any ICC calculation. This measurement has shown that the α_K values for both transitions do in fact agree with the modern Dirac-Fock ICC calculations with the atomic vacancy included.

Several years ago, our measurement of the 80.2-keV $M4$ transition in ^{193}Ir [5,6] was the first to show definitively that the atomic vacancy was required, at least in the case of low-energy ($\sim$4 keV) K-conversion electrons. The transitions in ^{134}Cs and ^{137}Ba now represent the first test among lighter nuclei and for transitions with significantly higher energy conversion electrons. By confirming our earlier conclusions, the present result supports the contention that the Dirac-Fock approach, including provision for the atomic vacancy, provides the best available ICC calculation over a large range of atomic numbers.

ACKNOWLEDGMENTS

The work of the Texas A&M authors is supported by the US Department of Energy under Grant no. DE-FG03-93ER40773 and by the Robert A. Welch Foundation under Grant no. A-1397. The work of M.T. is supported by the Russian Foundation for Basic Research under Grant no. 05-02-17340.

[1] S. Raman, T. A. Walkiewicz, R. Gunnink, and B. Martin, Phys. Rev. C **7**, 2531 (1973).
[2] R. S. Hager and E. C. Seltzer, Nucl. Data Tables A **4**, 1 (1968).
[3] S. Raman, C. W. Nestor, Jr., A. Ichihara, and M. B. Trzhaskovskaya, Phys. Rev. C **66**, 044312 (2002); See also the electronic addendum to this paper, the location of which is given in the paper's Ref. 32.
[4] I. M. Band, M. B. Trzhaskovskaya, C. W. Nestor, Jr., P. Tikkanen, and S. Raman, At. Data Nucl. Data Tables **81**, 1 (2002).
[5] N. Nica, J. C. Hardy, V. E. Iacob, S. Raman, C. W. Nestor, Jr., and M. B. Trzhaskovskaya, Phys. Rev. C **70**, 054305 (2004).
[6] N. Nica, J. C. Hardy, V. E. Iacob, J. R. Montague, and M. B. Trzhaskovskaya, Phys. Rev. C **71**, 054320 (2005).

[7] N. Nica, J. C. Hardy, V. E. Iacob, W. E. Rockwell, and M. B. Trzhaskovskaya, Phys. Rev. C **75**, 024308 (2007).
[8] J. H. Hubbell, P. N. Trehan, N. Singh, B. Chand, D. Mehta, M. L. Garg, R. R. Garg, S. Singh, and S. Puri, J. Phys. Chem. Ref. Data **23**, 339 (1994).
[9] E. Schönfeld and H. Janssen, Nucl. Instrum. Methods Phys. Res. A **369**, 527 (1996).
[10] J. C. Hardy, V. E. Iacob, M. Sanchez-Vega, R. T. Effinger, P. Lipnik, V. E. Mayes, D. K. Willis, and R. G. Helmer, Appl. Radiat. Isot. **56**, 65 (2002).
[11] R. G. Helmer, J. C. Hardy, V. E. Iacob, M. Sanchez-Vega, R. G. Neilson, and J. Nelson, Nucl. Instrum. Methods Phys. Res. A **511**, 360 (2003).
[12] R. G. Helmer, N. Nica, J. C. Hardy, and V. E. Iacob, Appl. Radiat. Isot. **60**, 173 (2004).
[13] T. W. Burrows, Nucl. Data Sheets **92**, 623 (2001).
[14] S. Raman, M. Ertugrul, C. W. Nestor, Jr., and M. B. Trzhaskovskaya, At. Data Nucl. Data Tables **92**, 207 (2006).
[15] D. Radford, http://radware.phy.ornl.gov/main.html, and private communication.
[16] Evaluated Nuclear Structure Data File maintained by the National Nuclear Data Center, Brookhaven National Laboratory: http://www.nndc.bnl.gov.
[17] C. T. Chantler, K. Olsen, R. A. Dragoset, J. Chang, A. R. Kishore, S. A. Kotochigova, and D. S. Zucker, X-Ray Form Factor, Attenuation and Scattering Tables (version 2.1), 2005. Available online at http://physics.nist.gov/ffast.
[18] J. A. Halbleib and T. A. Mehlhorn, Nucl. Sci. Eng. **92**, 338 (1986).